International Journal of Nanoelectronics and Materials
IJNeaM
ISSN 1985-5761 | E-ISSN 2232-1535

Insertion Loss Reduction in SAW Device through ZnO Nanoparticle Coating toward Cell Migration Applications

Mazlee Mazalan[a,*], Mohd Hafizuddin Junaidi[a], A. A. M. Ezanuddin[b], Liew Hui Fang[c], Muhammad Salman Al Farisi[d], Do Tien Dung[e], Mohd Fairus Ahmad[a], Anas Mohd Noor[a], Wan Safwani Wan Kamarulzaman[f], and Yufridin Wahab[a]

[a]*Centre of Excellence for Micro System Technology (MiCTEC), Faculty of Electronic Engineering & Technology, Universiti Malaysia Perlis, 02600 Arau, Perlis, Malaysia*
[b]*Faculty of Engineering and Built Environment, Lincoln University College, 47301 Petaling Jaya, Selangor, Malaysia*
[c]*Faculty of Electrical Engineering & Technology, Universiti Malaysia Perlis (UniMAP), 02600 Arau, Perlis, Malaysia*
[d]*Graduate School of Life Science and Systems Engineering, Kyushu Institute of Technology, Kitakyushu 808-0196, Japan*
[e]*Faculty of Information Technology 1, Posts and Telecommunication Institute of Technology, Ha Dong, Hanoi, Vietnam*
[f]*Department of Pharmaceutical Life Sciences, Faculty of Pharmacy, Universiti Malaya, Kuala Lumpur, Malaysia*
**Corresponding author. E-mail: mazleemazalan@unimap.edu.my*

Received 18 Aug 2025, Revised 12 May 2026, Accepted 21 May 2026

ABSTRACT

Surface acoustic waves (SAW) have been widely utilized for particle manipulation and cell migration due to their high efficiency and non-invasive nature. However, the presence of cell media and PDMS-based confined area can lead to significant insertion loss, which limits their effectiveness in biological applications. In this study, we explored the use of a ZnO nanoparticles to enhance the performance of SAW devices by reducing insertion loss for cell migration applications. Prior to fabrication, simulations were conducted to analyze the effect of the ZnO nanoparticles on the interdigital transducer (IDT). Prior to fabrication, COMSOL Multiphysics simulations showed that incorporating a ZnO layer improved in signal reflection by a 42% reduction, yielded an 18.3-fold increase in maximum surface displacement, and reduced localized mechanical stress by ~26.7%. The SAW devices were fabricated using standard microfabrication techniques, with ZnO nanoparticles deposited via sol-gel spin coating. Before depositing ZnO on IDT, the ZnO nanoparticle characteristics were confirmed by UV-Vis spectroscopy. After ZnO coating, the surface morphology was revealed by surface profiler and scanning electron microscopy (SEM). The measurement of transmission coefficient using a vector network analyzer (VNA) demonstrated approximately 80% reduction (10.06 dB) in magnitude as compared to the uncoated device. These results confirmed that the ZnO coating improves acoustic wave generation significantly and its potential for cell migration stimulation.

Keywords: *Surface acoustic wave; ZnO nanoparticles; insertion loss; interdigital transducer; cell migration; electromechanical coupling*

1. INTRODUCTION

Essential biological events, such as wound closure and the devastating spread of cancer, share a common requirement: cells must move with high directional accuracy [1]. To learn this "steering," researchers have had to get innovative with how they apply force to the cells. In vascular biology, for instance, the focus is often on fluid shear stress, as it is the only reliable way to mimic the hydrodynamic drag within a blood vessel [2]. Cyclic stretching is usually used on "stretchy" tissues, such as the lungs or muscles, which target mechanotransduction pathways associated with physical tugging [3]. Different to physical pressure, some groups used voltage gradients or electrotaxis to guide cells during skin repair [4], while other groups applied the magnetic fields to remote position nanoparticle-labeled cells with high spatial precision [5].

Acoustic wave stimulation has emerged as a strong alternative to traditional mechanical methods, largely because it avoids direct physical contact. When high-frequency vibrations move across a piezoelectric substrate, SAW platforms create highly localized pressure fields in the fluid above them. The main advantage here is precision. Since the waves manipulate the biological sample without touching it, SAW setups bypass the physical barriers typical of other techniques [6]. The underlying biology is just as important. So far, only a few studies have been done to manipulate SAW onto biological samples. For example, research done by Imashiro and colleagues showed that these acoustic propagating waves do more than just physically push cells around. Instead, the cells convert those surface vibrations into internal biochemical cues that drive migration through mechanotransduction [8]. Building on this concept, Brugger's team integrated these SAW mechanisms directly into microfluidic chips. By utilizing standing wave patterns, they managed to achieve completely contactless cell positioning [9].

Despite these advances, a persistent challenge remains in biological settings: the cell culture medium and PDMS-based enclosures introduce significant insertion loss [7], attenuating acoustic energy before it reaches the cells. Simply increasing the input RF power is not a practical solution because higher power levels lead to excessive heat generation, which risks substrate degradation and cell damage. ZnO-based coatings offer a more targeted solution. Zakaria et al. reported improved SAW sensor sensitivity with ZnO nanowires [10], and Hao et al. observed that ZnO layers on $LiNbO_3$ substrates enhance electrical characteristics and acoustic performance [11]. Motivated by these findings, this study aims to deposit a ZnO nanoparticle layer directly onto the IDTs of a $LiNbO_3$-based SAW device and quantify the resulting reduction in insertion loss, with the longer-term objective of enabling more efficient, low-power acoustic stimulation of migrating cells.

2. MATERIALS AND METHODS

2.1 Device Architecture

Before fabrication, numerical simulations were performed at a fixed resonance frequency of 124 MHz using COMSOL Multiphysics 5.6. This frequency was not arbitrarily chosen; it is determined directly by the IDT geometry, as the resonance frequency equals the acoustic wave velocity of the substrate divided by the spatial wavelength defined by the IDT finger spacing [9]. The IDT geometry and substrate cut were specifically optimized to deliver adequate acoustic energy to the biological medium while limiting heat generation, and 124 MHz is the natural resonant frequency for this configuration.

The SAW device consists of IDTs patterned on a 128° YX-cut $LiNbO_3$ substrate, selected for its high acoustic propagation velocity and strong electromechanical coupling coefficient. Aluminum (Al) was used for the IDT electrodes due to its low electrical resistivity and processing compatibility. The $LiNbO_3$ substrate thickness was 250 µm, and the Al layer was 200 nm thick. Key device dimensions are summarized in Table 1. Boundary conditions fixed the left, right, and bottom faces of the substrate to suppress reflections, while the top surface was left free to observe wave propagation (Figure 2a). The mesh comprised edge and mapped elements for the substrate, free triangular elements for the cell medium region, and free quad elements for the IDT (Figure 2b). Frequency-response analysis extracted the von Mises stress distribution (Figure 2c), S_{11} reflection coefficient, and maximum surface displacement. The ZnO coating was modeled as a 600 nm layer over both the $LiNbO_3$ substrate and IDTs, with material properties derived from published literature [13], while $LiNbO_3$ and Al properties followed our prior work [14].

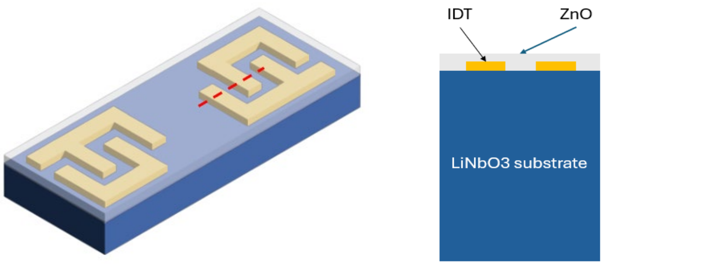

(a) (b)

Figure 1. Structure of the SAW device, (a) 3D structure where the dotted red line shows the cross-section for (b) 2D structure.

Table 1 Key dimensions of the SAW device

Parameter	Value
Frequency, f	124 MHz
Delay line, d	7 mm
ZnO layer thickness	600 nm
$LiNbO_3$ substrate thickness	250 µm
Al electrode thickness	200 nm

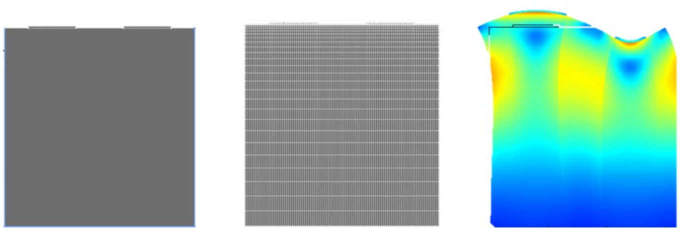

(a) (b) (c)

Figure 2. Simulation steps (a) the left, right, and bottom sides of the $LiNbO_3$ substrate is fixed, (b) mesh setting, and frequency analysis on von Mises stress of LiNBo3 substrate.

2.2 Experimental Procedure

Device fabrication followed a standard microfabrication sequence. A 200 nm Al film was first thermally evaporated onto the $LiNbO_3$ substrate (Figure 3a), followed by photolithography and wet chemical etching to define the IDT finger pattern (Figure 3b). A thin SiO_2 passivation layer was then deposited to ensure biocompatibility with live cells (Figure 3c).

ZnO nanoparticles were deposited via a sol-gel process using zinc acetate dihydrate as the precursor, with precise weighing (Figure 4a). In an alcoholic solution, zinc acetate dihydrate dissociates into zinc monoacetate and acetate ions (Figure 4b), water molecules and acetate ions subsequently adsorb onto the substrate surface.

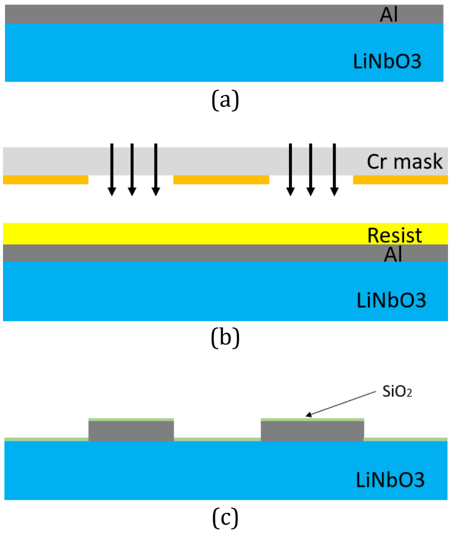

Figure 3. Fabrication process of the SAW device (a) Al deposition, (b) photolithography process, and (c) Al etching and SiO2 deposition.

Hydrolysis of zinc monoacetate generates zinc oxide and acetic acid; because the drying step was performed at 150 °C—above the boiling point of acetic acid (118 °C)—the acid evaporates, leaving ZnO behind. Ethanolamine was used as a chelating and stabilizing agent to prevent premature $Zn(OH)_2$ precipitation and promote cross-linking between zinc atoms.

The precursor solution was spin-coated onto the IDT surface at 500 rpm for 40 s (Figure 4c). The coated substrate was soft-baked at 110 °C for 1 min to remove residual organics. This spin-coat–bake cycle was repeated six times to achieve the target film thickness (Figure 4d), followed by furnace annealing at 500 °C for 5 h to densify the film. The ZnO solution was verified by UV-Vis spectroscopy (Lambda 950 UV-Vis/NIR Spectrometer) before deposition, and surface morphology was characterized by scanning electron microscopy (HITACHI/TM4000PLUS II). Electrical performance (S_{21}) was measured using a Rohde & Schwarz ZVL vector network analyzer (VNA) using the setup as shown in Figure 5.

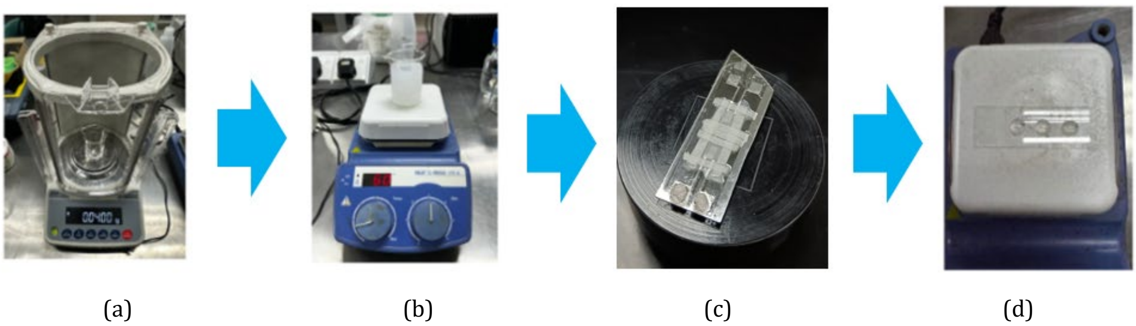

Figure 4. Coating process of ZnO nanoparticles on the IDT of SAW device (a) weighting process of precursor materials, (b) precursor is dissolved in ethanolamine, (c) coating process, and (d) soft-baking process.

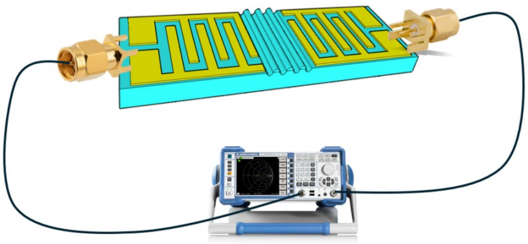

Figure 5. Experiment setup for validation of piezoelectric effect and S21.

3. RESULTS AND DISCUSSION

3.1 Simulation Analysis

The simulation was configured to extract the reflection coefficient S_{11} because the setup could not directly compute insertion loss S_{21}. However, S_{11} and S_{21} are physically linked through energy conservation in a passive two-port network. For a SAW device, incident wave energy divides strictly into transmitted, reflected, and absorbed components, yielding the relation $|S_{11}|^2 + |S_{21}|^2 + P\_loss = 1$, where P_loss accounts for material absorption, scattering, and propagation losses [15]. A reduction in S_{11}, therefore, directly implies improved energy transfer to the acoustic mode.

For the bare device (without ZnO), the von Mises stress plot (Figure 6a) shows a peak stress near the IDT fingers of approximately 3×10^5 N/m^2, consistent with energy concentration at the electrode edges in bare piezoelectric devices. The S_{11} response (Figure 6b) shows a dip to −19 dB at 130 MHz, corresponding to the resonance frequency of most efficient energy coupling. The maximum surface displacement (Figure 6c) peaks at ~60×10^{-7} µm at 130 MHz.

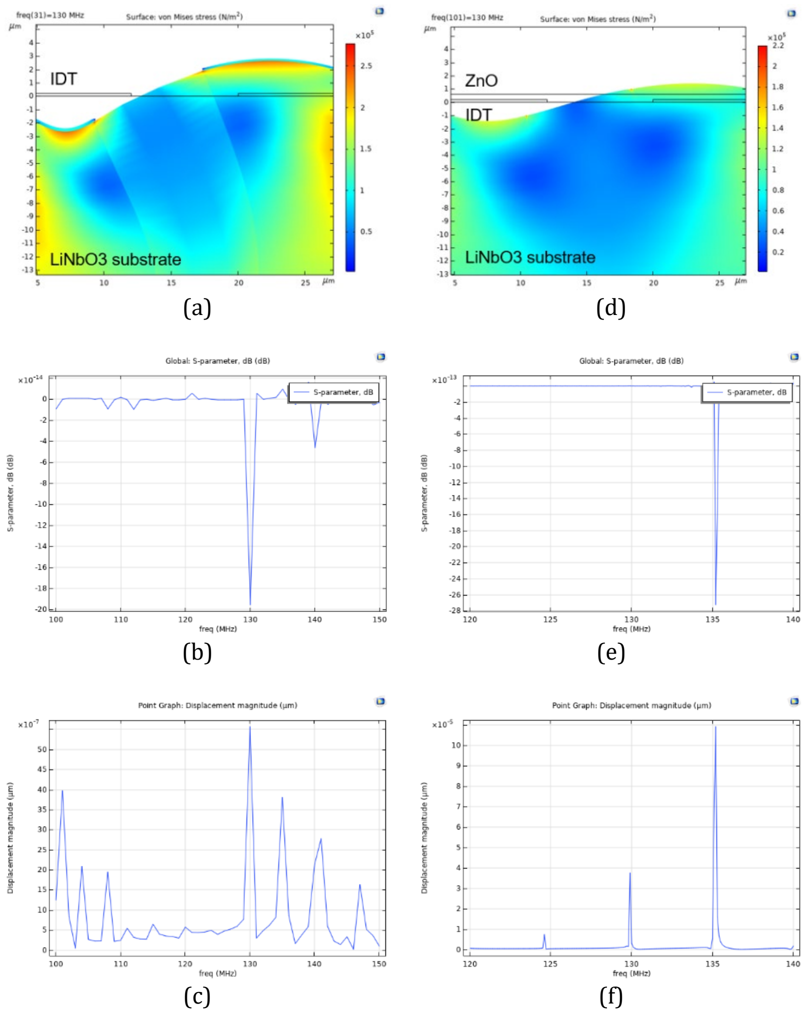

Figure 6. Comparison of SAW device performance without and with a ZnO layer on the IDT. (a–c) Device without ZnO: (a) von Mises stress distribution, (b) reflection coefficient (S11), and (c) surface displacement magnitude. (d–f) Device with ZnO layer: (d) von Mises stress distribution, (e) reflection coefficient (S11), and (f) surface displacement magnitude.

With the 600 nm ZnO coating (Figures 6d–f), the peak von Mises stress drops to ~2.2×10^5 N/m^2, a ~26.7% reduction, attributed to the ZnO film distributing acoustic energy more uniformly. The S_{11} dip deepens to −27 dB at ~135 MHz, representing an 8 dB improvement (~42% reduction in reflected power). Most strikingly, the maximum surface displacement increases to ~11×10^{-5} μm—an 18.3-fold enhancement over the uncoated device—driven by the added piezoelectric contribution of ZnO, reinforcing the electromechanical conversion of the $LiNbO_3$ substrate. Together, these results confirm that ZnO simultaneously improves energy transfer efficiency, amplifies acoustic displacement, and redistributes mechanical stress more uniformly.

3.2 Experimental Results

Before deposition, UV-Vis spectroscopy of the ZnO precursor solution (Figure 7) revealed a sharp absorption edge at 378 nm with peak absorbance of 10.45 AU, consistent with the bandgap of stoichiometric ZnO (~3.3–3.4 eV, absorption edge ~370–380 nm) [14,15], confirming successful ZnO nanoparticle formation.

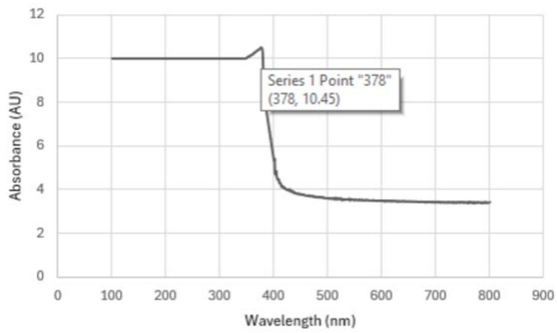

Figure 7. Absorbance of ZnO solution measured using UV-Vis spectrophotometer.

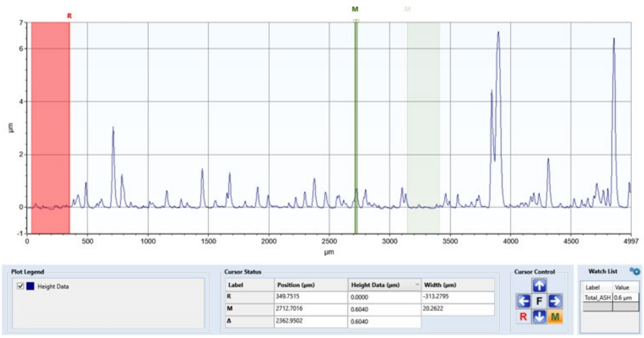

Figure 8. Thickness of ZnO nanoparticles on SAW device.

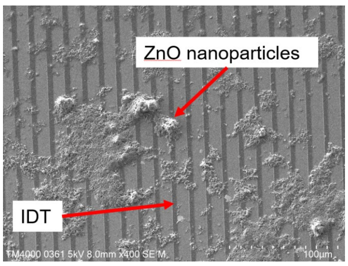

Figure 9. ZnO nanoparticles on IDT of SAW device.

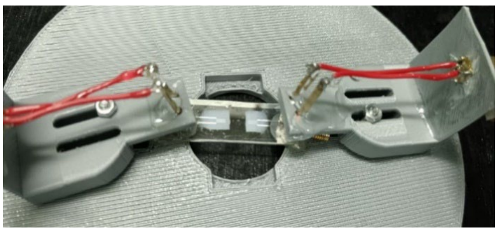

Figure 10. SAW devices on customize RF probe station (white spot on IDTs can be seen in red circle indicated ZnO layer).

Surface profilometry (Figure 8) indicated a spatially non-uniform film with an average thickness of ~600 nm—in good agreement with the simulation model—with non-uniformity attributed to rapid solvent evaporation during spin coating. SEM imaging (Figure 9) confirmed ZnO deposition on the IDT structures and revealed nanoparticle clustering consistent with profilometer data. While non-uniformity is generally undesirable, in biological applications the variation in mass loading creates a distributed resonance response that may benefit stimulation of heterogeneous cell populations.

Figure 11 compares S_{21} responses. The uncoated device (Figure 11a) shows a resonance peak at 143.4 MHz with an insertion loss of −22.63 dB, reflecting weak electromechanical coupling of the bare $LiNbO_3$/Al system. After ZnO deposition (Figure 11b), the resonance sharpens and shifts to 140.1 MHz, with insertion loss reduced to −12.57 dB. The 10.06 dB improvement corresponds to ~80% reduction in reflection coefficient magnitude. The frequency downshift from 143.4 to 140.1 MHz is consistent with the mass loading effect: the ZnO film increases mass per unit area, reducing surface acoustic wave velocity and shifting resonance to a lower frequency. Changes in elastic and piezoelectric properties of the composite stack also contribute. The sharper, more distinct resonance peak in Figure 11(b) reflects improved acoustic confinement and reduced scattering losses, consistent with simulation predictions.

The ~10 dB improvement achieved by simple ZnO spin coating compares favorably with more complex strategies. Grooved reflective grating structures on ZnO films reportedly reduce insertion loss from −47.9 dB to −19.49 dB [17], a significant improvement but one requiring additional micro-machining steps. Our approach achieves a comparable enhancement solely through direct deposition of ZnO nanoparticles. This is consistent with work by Augustine et al., who demonstrated reduced insertion loss in electrospun P(VDF–TrFE)/ZnO composite-coated SAW devices [18]. The mechanism—improved K^2 from ZnO integration—is supported by Fu et al., who showed that optimizing ZnO layer properties leads to stronger acoustic wave generation and lower signal loss [19]. Regarding biological implications, SAW devices with lower insertion loss deliver more acoustic energy to the cell medium, generating leaky waves that exert mechanical forces on cells. These forces act on the cell membrane and cytoskeleton, potentially enhancing cell motility, reorienting migration direction, or triggering mechanotransduction responses [9].

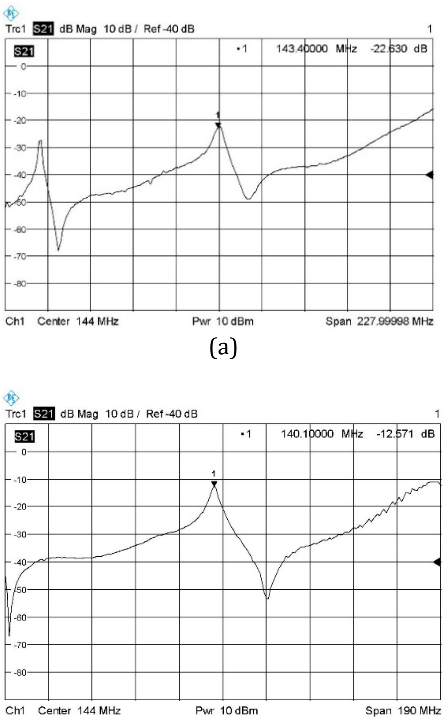

Figure 11. Transmission response (S_{21}) of (a) SAW device without a ZnO layer and (b) SAW device with a ZnO layer on the IDT.

CONCLUSION

In this study, the ZnO nanoparticles layer has been successfully deposited on IDT of the SAW devices. This is confirmed by observation and measurement using a surface profiler, SEM, and UV-Vis spectroscopy. Applying the ZnO nanoparticle layer via a standard sol-gel spin-coating method has been shown to be highly effective at reducing insertion loss. Initial modelling in COMSOL showed an increase in S_{11} by 8 dB alongside an 18.3-fold boost in surface displacement, while also reducing the localized stress concentration by approximately 26.7%. To validate these models physically, we conducted a real experiment in which we performed electrical measurements using a VNA. As a result, it recorded a 10.06 dB drop in insertion loss (essentially an 80% cut in reflected power. It must be said that by adding mass to the device caused the operating frequency to drift from 124 MHz up to about 140 MHz due to the mass-loading effect, which is a standard hurdle in coating strategies—and one we will need to account for in future design iterations—the sheer gain in overall acoustic output makes the compromise worthwhile. Moving forward, the future work may take this optimized energy delivery and test it biologically. We plan to run in vitro assays to assess how effectively this platform can deliver mechanical stimulation and govern cell migration behaviour.

ACKNOWLEDGMENTS

The authors gratefully acknowledge the Ministry of Higher Education (MOHE) for financial support under the Fundamental Research Grant Scheme, FRGS/1/2024/TK07/UNIMAP/03/4.

REFERENCES

[1] M. Bin Mazalan, M. A. Bin Ramlan, J. H. Shin, and T. Ohashi, "Effect of geometric curvature on collective cell migration in tortuous microchannel devices," Micromachines, vol. 11, no. 7, pp. 1–17, 2020.

[2] P. A. Galie, A. van Oosten, C. S. Chen, and P. A. Janmey, "Application of multiple levels of fluid shear stress to endothelial cells plated on polyacrylamide gels," Lab Chip, vol. 15, no. 4, pp. 1205–1212, 2015.

[3] C. Argentati et al., "Insight into mechanobiology: How stem cells feel mechanical forces and orchestrate biological functions," Int. J. Mol. Sci., vol. 20, no. 21, 2019.

[4] G. Tai, M. Tai, and M. Zhao, "Electrically stimulated cell migration and its contribution to wound healing," Burn. Trauma, vol. 6, pp. 1–7, 2018.

[5] S. Yaman, M. Anil-Inevi, E. Ozcivici, and H. C. Tekin, "Magnetic force-based microfluidic techniques for cellular and tissue bioengineering," Front. Bioeng. Biotechnol., vol. 6, no. DEC, 2018.

[6] C. Devendran, J. Carthew, J. E. Frith, and A. Neild, "Cell adhesion, morphology, and metabolism variation via acoustic exposure within microfluidic cell handling systems," Adv. Sci., vol. 6, no. 24, 2019.

[7] Z. Tian et al., "Generating multifunctional acoustic tweezers in Petri dishes for contactless, precise manipulation of bioparticles," Sci. Adv., vol. 6, no. 37, 2020.

[8] C. Imashiro et al., "Propagating acoustic waves on a culture substrate regulate the directional collective cell migration," Microsystems Nanoeng., vol. 7, no. 1, 2021.

[9] M. S. Brugger et al., "Vibration enhanced cell growth induced by surface acoustic waves as in vitro wound-healing model," Proc. Natl. Acad. Sci. U.S.A., vol. 117, no. 50, pp. 31603–31613, 2020.

[10] M. R. Zakaria, S. F. A. Rahman, S. Lleng, M. H. Mat, and U. Hashim, "Modification of surface acoustic wave (SAW) sensor using zinc oxide nanowires," Int. J. Nanoelectron. Mater., vol. 11, pp. 33–42, 2018.

[11] L. Hao et al., "Fabrication and electrical properties of LiNbO3/ZnO/n-Si heterojunction," AIP Adv., vol. 3, no. 4, 2013.

[12] M. Mazalan et al., "Design and fabrication of surface acoustic wave (SAW) device for cell migration control," in 4th Int. Conf. Innovation Biomed. Eng. Life Sci., 2024, pp. 114–125.

[13] K. Arun, M. S. Lekshmi, and K. J. Suja, "Design and simulation of ZnO based acetone gas sensor using COMSOL Multiphysics," in Proc. 2020 7th Int. Conf. Signal Process. Integr. Networks (SPIN), 2020, pp. 659–662.

[14] M. Bin Mazalan, A. M. Noor, Y. Wahab, S. Johari, M. R. Zakaria, and W. S. W. K. Zaman, "A numerical study of collective cell migration in a microchannel driven by surface acoustic wave (SAW) device," J. Phys. Conf. Ser., vol. 2550, no. 1, 2023.

[15] P. E. Timoshenko, V. V. Kalinchuk, and V. B. Shirokov, "Finite-element analysis of scattering parameters of surface acoustic wave bandpass filter formed on barium titanate thin film," Int. J. Smart Nano Mater., vol. 9, no. 2, pp. 88–98, 2018.

[16] A. Khorsand Zak, R. Razali, W. H. Abd Majid, and M. Darroudi, "Synthesis and characterization of a narrow size distribution of zinc oxide nanoparticles," Int. J. Nanomedicine, vol. 6, no. 1, pp. 1399–1403, 2011.

[17] K. Lange, F. J. Gruhl, and M. Rapp, "Surface acoustic wave (SAW) biosensors: Coupling of sensing layers and measurement," Methods Mol. Biol., vol. 949, pp. 491–505.

[18] R. Augustine, F. Sarry, N. Kalarikkal, S. Thomas, L. Badie, and D. Rouxel, "Surface acoustic wave device with reduced insertion loss by electrospinning P(VDF–TrFE)/ZnO nanocomposites," Nano-Micro Lett., vol. 8, no. 3, pp. 282–290, 2016.

[19] S. Fu et al., "High-frequency V-doped ZnO/SiC surface acoustic wave devices with enhanced electromechanical coupling coefficient," Appl. Phys. Lett., vol. 114, no. 11, 2019.